Explicit Wave function of the Interacting Non-Hermitian Spin-1/2 1D System

Yue Wang,[1,2] Xiangyu Zhang,[2] Zhesen Yang,[3,*] and Congjun Wu[2,4,5,6,†]
[1]Department of Physics, Zhejiang University, Hangzhou 310027, China
[2]New Cornerstone Science Laboratory, Department of Physics, School of Science, Westlake University, Hangzhou 310024, Zhejiang, China
[3]Department of Physics, Xiamen University, Xiamen 361005, Fujian Province, China
[4]Institute for Theoretical Sciences, Westlake University, Hangzhou 310024, Zhejiang, China
[5]Key Laboratory for Quantum Materials of Zhejiang Province, School of Science, Westlake University, Hangzhou 310024, Zhejiang, China
[6]Institute of Natural Sciences, Westlake Institute for Advanced Study, Hangzhou 310024, Zhejiang, China

(Received 20 September 2024; revised 5 August 2025; accepted 16 December 2025; published 20 January 2026)

We present an explicit Bethe-ansatz wave function to a 1D spin-1/2 interacting fermion system, manifesting a many-body resonance resulting from the interplay between interaction and non-Hermitian spin-orbit coupling. In the dilute limit, the Bethe-ansatz wave function is factorized into Slater determinants and a Jastrow factor. An effective thermodynamic distribution is constructed with an effective Hamiltonian including a repulsion resulting from Pauli's exclusion principle and a distinctive zigzag potential arising from the resonance. The competition between these effects leads to a transition from a uniformly distributed configuration to a phase separation. Clustering of particles with identical spins is observed in the latter phase, demonstrating that the many-body resonance effect is enhanced by the repulsive interaction.

DOI: 10.1103/bhpz-17d2

Introduction—The non-Hermitian skin effect (NHSE) has attracted significant attentions recently [1–8]. The associated exotic properties, such as the complex-valued spectrum and the localization on boundaries, can be described by the theory of the generalized Brillouin zone, in which momenta are complex valued [3,9–14]. These distinctive features are highly sensitive to boundary conditions. For example, the eigenstates in non-Hermitian systems are extended under the periodical boundary condition (PBC) while localized under the open boundary condition (OBC), which contrasts to the case in Hermitian physics. Experimentally, the NHSE has been observed in various systems, including metamaterials [15,16], photonic systems [17], electrical circuits [18,19], acoustic crystals [20], and cold atomic systems [21].

Despite the significant progress in the NHSE, current studies predominantly focus on the single-body physics. How the NHSE behaves under strong interactions remains an open question, and non perturbative analytical studies are desired. The Bethe-ansatz (BA) method [22,23] is a systematic tool for studying one-dimensional (1D) integrable systems, including the Lieb-Liniger model of the interacting Bose gas [24,25], the Gaudin-Yang model of the interacting Fermi gas [26,27], and the Lieb-Wu solution to the Hubbard model [28]. When applied to non-Hermitian systems [29–31], it has been found that NHSE is suppressed by repulsive interactions [32–36]. However, the complexity of BA wave functions makes it difficult to calculate observables. It would be desirable to construct an explicit many-body wave function to facilitate a deeper understanding of the NHSE in interacting systems, akin to the Ogata-Shiba-type and the Laughlin-type wave functions [37–39].

In this Letter, we present a concise expression for the many-body wave function in a 1D spin-1/2 fermion system with the non-Hermitian spin-orbit coupling (SOC). As a result of the repulsive δ interaction, each particle behaves as a soft boundary to particles with opposite spins, inducing an effective unidirectional attraction between them. Resonance states are formed here instead of bound states, i.e., the Bethe string states [40–42]. The explicit many-body wave function is constructed in the dilute limit, which is a rare example in many-body physics. It consists of the product of Slater determinants and the Jastrow factor [43] reflecting the resonance between particles with opposite spins. Remarkably, a phase transition occurs as the interacting strength increases, where the level of localization exhibits a jump, indicating that the resonance is enhanced by the repulsive interaction.

Model—We start with the following 1D non-Hermitian many-body Hamiltonian with system length L ($\hbar = 1$)

$$\hat{H} = \sum_{l=1}^{N} \frac{(-i\nabla_l + im\alpha\sigma_l^z)^2}{2m} + \sum_{l<l'} 2g\delta(x_l - x_{l'}), \quad (1)$$

*Contact author: yangzs@xmu.edu.cn
†Contact author: wucongjun@westlake.edu.cn

where $\alpha > 0$ and $g > 0$ represent the strength of the non-Hermitian SOC and the repulsive interaction respectively; the PBC is assumed. Since the z component of total spin is conserved, the eigenvalues and eigenstates can be labeled by the particle numbers of two components, i.e., $N_\uparrow$ and $N_\downarrow$. In the following, the real and imaginary parts of the complex momentum are defined as

$$k_{l,\sigma_l} = (\chi_{l,\sigma_l} + i\eta_{l,\sigma_l})/L, \tag{2}$$

where $\sigma_l = \pm 1$ represents the spin z component.

We warm up by considering the single-body problem. If the particle carries spin σ ($\sigma = \uparrow, \downarrow$), the eigenstates are denoted as $e^{ik_\sigma x}|\sigma\rangle$, and the eigenenergies are $(k_{\uparrow,\downarrow} \pm im\alpha)^2/(2m)$. The momentum is quantized as $k_\sigma = 2\pi n_\sigma/L$ under the PBC. Upon the OBC, the spin-up and down particles localize at the right and left boundaries, respectively. The single-particle localization length is $\lambda_s = (m\alpha)^{-1}$, which is independent of the system size, indicating the presence of bound states. This is the conventional NHSE discussed in the literature.

Two-body case—With $N_\uparrow = 2$ and $N_\downarrow = 0$, the corresponding eigenstate is a Slater determinant of plane wave states with $k_{i,\uparrow} = 2\pi n_{i,\uparrow}/L$ and $i = 1, 2$. The δ interaction does not manifest here due to Pauli's exclusion principle. The corresponding eigenenergy is $E = \sum_i (k_{i,\uparrow} + im\alpha)^2/2m$. The case with two spin-down particles can be constructed in parallel.

Nontrivial interaction effect emerges with a pair of particles of opposite spins. The eigenstate is written as $\varphi(x_1, x_2)|\downarrow\uparrow\rangle - \varphi(x_2, x_1)|\uparrow\downarrow\rangle$. Using the center of mass coordinate $X = (x_1 + x_2)/2$ and the relative coordinate $r = x_1 - x_2$, the wave function is decomposed as $\varphi(x_1, x_2) = \Phi(X)\phi(r)$, satisfying the following equations,

$$\begin{aligned} &\left(-\tfrac{\nabla_X^2}{4m} - m\alpha^2\right)\Phi(X) = E_X\Phi(X), \\ &\left(-\tfrac{\nabla_r^2}{m} - 2\alpha\nabla_r + 2g\delta(r)\right)\phi(r) = E_r\phi(r). \end{aligned} \tag{3}$$

$\Phi(X)$ is solved as $e^{iK_X X}$, where $K_X = 2\pi n_K/L$. The non-Hermitian term $-2\alpha\nabla_r$ only appears in the motion of the relative coordinate, where the δ potential acts as a soft boundary. As a result, the reminiscence of the NHSE would bring an effective unidirectional attraction between two particles, explained as follows. The relative motion is solved as

$$\phi(r) = Ae^{ik_r r} + Be^{-ik_r r - 2m\alpha r}, \tag{4}$$

where A, B are scattering amplitudes, $k_r = (\chi_r + i\eta_r)/L$ is the complex momentum. Matching wave functions on both sides of the δ potential, it yields,

$$\frac{\beta}{g}\left((-1)^{n_K}\cosh m\alpha L - \cosh m\beta L\right) = \sinh m\beta L, \tag{5}$$

where $\beta = \alpha + i(k_r/m)$. As shown in Supplemental Material (SM) Sec. I [44], in the case of $L \gg \lambda_s$, Eq. (5) is solved as

$$\begin{aligned} &\chi_r = (2n_r + n_K)\pi, \quad \eta_r = \ln\left(1 + \tfrac{g}{\alpha}\right), \\ &\tfrac{A}{B} = -\left(1 + \tfrac{\alpha}{g}\right). \end{aligned} \tag{6}$$

$\phi(r)$ is identical to a single-body wave function of spinless particle subjected to a "soft" boundary condition, which lies between the cases of OBC and PBC, since the δ potential permits partial transmission. In all cases, the solution possesses a pair of momenta, whose imaginary parts are summed to $2m\alpha$. In the OBC case, both imaginary parts equal $m\alpha$, while in the PBC case, one becomes real and the other carries the imaginary part of $2m\alpha$. In our case, a small imaginary part η_r/L is at the order of $1/L$, and the other remains at the order of $2m\alpha$. Consequently, the decay of $\phi(r)$ is at the length scale of L, such that these states are resonance rather than bound states [45,46]. The situation of OBC is recovered for $g \sim (1/mL)e^{L/\lambda_s}$ in which case the localization length $L/\eta_r \sim \lambda_s$, while that of PBC corresponds to $g = 0$.

In the lab frame, $\varphi(x_1, x_2)$ is written as

$$\begin{aligned} &\theta(x_1 > x_2)\left(Ae^{i(k_{1,\downarrow}x_1 + k_{2,\uparrow}x_2)} + Be^{i(k_{2,\downarrow}x_1 + k_{1,\uparrow}x_2)}\right) \\ &+\theta(x_2 > x_1)\left(A'e^{i(k_{1,\downarrow}x_1 + k_{2,\uparrow}x_2)} + B'e^{i(k_{2,\downarrow}x_1 + k_{1,\uparrow}x_2)}\right), \end{aligned} \tag{7}$$

where $0 < x_{1,2} < L$. B and B' terms are the reflected waves of A and A' terms, respectively. After the reflection, the real parts of momenta switch, but their imaginary parts change due to the SOC. As a result, the imaginary parts of $k_{1,\downarrow}$ and $k_{2,\uparrow}$ are at the order of $1/L$,

$$k_{1,\downarrow} = (\chi_1 + i\eta_r)/L, \qquad k_{2,\uparrow} = (\chi_2 - i\eta_r)/L, \tag{8}$$

while that of the reflected momenta $k_{1,\uparrow}$ and $k_{2,\downarrow}$ become finite as

$$k_{1,\uparrow} = k_{1,\downarrow} - 2im\alpha, \qquad k_{2,\downarrow} = k_{2,\uparrow} + 2im\alpha. \tag{9}$$

Here $\chi_i = 2\pi n_i$ with $i = 1, 2$. A' and B' terms are the transmitted waves of A and B terms, respectively. The PBC yields $A'/A = e^{ik_{1,\downarrow}L}$ and $B'/B = e^{ik_{2,\downarrow}L}$.

We view A, A' terms as the incident waves and B, B' terms as the reflected waves. Since the imaginary parts of their momenta behave differently, in the case of $L \gg \lambda_s$, the reflected waves can be dropped if the interparticle distance exceeds λ_s. Then the wave function is simplified to the product of plane waves and a Jastrow factor,

$$\varphi(x_1, x_2) = Ae^{i(\chi_1 x_1 + \chi_2 x_2)/L} \cdot e^{-\frac{1}{2}W(x_1 - x_2)}, \tag{10}$$

where $e^{-\frac{1}{2}W(x_1-x_2)}$ is given by the sum of step functions modified by the imaginary parts of the complex momenta

$$e^{-\eta_r(x_1-x_2)/L}\left(\theta(x_1 > x_2) + \theta(x_2 > x_1)\left(1 + \frac{g}{\alpha}\right)^{-1}\right).$$

More explicitly,

$$W(r) = 2\eta_r\left(\frac{r}{L} + \theta(-r)\right), \qquad -L < r < L. \tag{11}$$

The exact and approximated wave functions Eqs. (7) and (10) are shown in Fig. 1. The spin-up particle is fixed at $x_2 = 0$. Increasing x_1 from 0, $\varphi(x_1, x_2)$ rapidly reaches the peak located at $x_{1,\text{peak}} \sim \ln(L\lambda_s^{-1})/(L\lambda_s^{-1})$. If $L \gg \lambda_s$, $x_{1,\text{peak}}$ coincides with x_2. The peak is followed by a slow decay at the length scale of L, which means the spin-down particle prefers the right side of the spin-up one. This can be understood as a weaker version of the NHSE with localization length L/η_r. Note that this length decreases as g increases, indicating that the localization is enhanced by the repulsive interaction, which distinguishes it from the conventional NHSE suppressed by repulsions as reported in the previous studies [32–36]. The behavior at $x_1 < 0$ can be obtained by applying the PBC. As we will explain later,

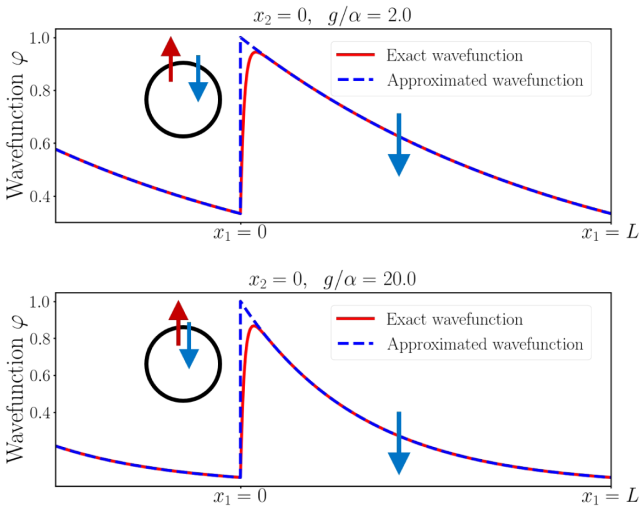

FIG. 1. The two-body wave function $\varphi(x_1, x_2)$ with particles of opposite spins by fixing the spin-up one at $x_2 = 0$. The parameter values are $\chi_1 = \chi_2 = 0$, $m = 1$, $\alpha = 1$ and $L = 50$. The peak appears at $x_1 \sim \ln(L\lambda_s^{-1})/(L\lambda_s^{-1})$. In the case of $L \gg \lambda_s$, the peak is located at $x_1 = x_2$ and φ becomes discontinuous. It implies that the spin-down particle tends to lie on the right side of the spin-up particle, forming a resonant pair on the ring. The wave function becomes more localized as the strength of repulsive interaction g increases, which indicates that the resonance is enhanced by the repulsive interaction.

the two-body wave function can be generalized to the many-body case where the above picture still holds.

Many-body problem: BA equations—For eigenstates with $N_\downarrow$ down spins and $N_\uparrow = N - N_\downarrow$ up spins, the corresponding BA equations are

$$\prod_{i=1}^{N_\downarrow} \frac{\Lambda_i - \bar{k}_l - img}{\Lambda_i - \bar{k}_l + img} = e^{i\bar{k}_l L} e^{m\alpha L},$$
$$\prod_{l=1}^{N} \frac{\Lambda_i - \bar{k}_l - img}{\Lambda_i - \bar{k}_l + img} = -e^{2m\alpha L} \prod_{i'=1}^{N_\downarrow} \frac{\Lambda_i - \Lambda_{i'} - 2img}{\Lambda_i - \Lambda_{i'} + 2img}, \tag{12}$$

where $\{\bar{k}_l\}$ and $\{\Lambda_i\}$ are N and $N_\downarrow$ variables to be determined, with $1 \le l \le N$ and $1 \le i, i' \le N_\downarrow$. Once $\{\bar{k}_l\}$ are obtained, the corresponding momentum of the lth particle with spin σ_l is given by

$$k_{l,\sigma_l} = \bar{k}_l - im\alpha\sigma_l. \tag{13}$$

Note that the scattering is always nondiffractive in terms of $\bar{k}_l$, which ensures the integrability of the model.

The solutions to BA equations are significantly simplified due to the non-Hermitian SOC. For example, in the two-body case, the solutions can be effectively expressed by Eq. (8), since those reflected waves with momenta $\{k_{1,\uparrow}, k_{2,\downarrow}\}$ are removed in the approximation to the wave functions. The same thing happens in the many-body case. As illustrated in Fig. 2, the many-body wave function is composed of many "plane waves," connected with each other by scattering. Those "plane waves" in the same column are connected by transmission, which share the same momenta since transmission exchanges the positions of the particles while preserving their momenta. For example, $A_2, A_3 \cdots$ are the transmission descendants of A_1, with momenta

$$k_{i,\downarrow} = (\chi_i + i\eta_r N_\uparrow)/L, \qquad k_{j,\uparrow} = (\chi_j - i\eta_r N_\downarrow)/L. \tag{14}$$

Here $1 \le i \le N_\downarrow$, $N_\downarrow + 1 \le j \le N$, $\chi_l = 2\pi n_l$, and η_r is defined in Eq. (6). $A_1, A_2, A_3 \cdots$ are denoted as incident waves, like the A and A' terms in the two-body case. Each incident wave has many reflected descendants, aligned in the same row. Due to the diffractive reflection described by Eq. (9), these descendants decay much faster than the incident waves, and therefore can be discarded in the dilute limit defined as

$$\frac{d}{\lambda_s} \gg \ln\left(1 + \frac{g}{\alpha}\right), \tag{15}$$

where $d = L/N$ is the average interparticle distance. Detailed calculations are found in SM Sec. II [44]. Note that our approximated solution exhibits a singularity at $\alpha = 0$, since the dilute limit is broken in that case.

Comparing Eq. (14) with the two-body solution Eq. (8), one finds that only imaginary parts of momenta change, which are amplified by the number of particles with opposite spins. This fact stems from the nature of resonant states. For a spin-down particle, it deems each spin-up particle as a soft boundary, such that its length free of collision is roughly $L/N_\uparrow$. Hence, the imaginary part of $k_{i,\downarrow}$ in Eq. (14) is amplified by a factor of $N_\uparrow$. The case for a spin-up particle is in parallel.

BA wave functions—We denote $\varphi(x_\downarrow; x_\uparrow)$ as an abbreviation to the following wave function:

$$\varphi_{\underbrace{\downarrow\downarrow\cdots\downarrow}_{N_\downarrow}\underbrace{\uparrow\uparrow\cdots\uparrow}_{N_\uparrow}}(x_1, x_2 \cdots x_{N_\downarrow}; x_{N_\downarrow+1}, x_{N_\downarrow+2} \cdots x_N).$$

Other spin configurations of the BA wave function can be obtained by permutations according to Fermi statistics.

In general, the BA wave function is very complex. Fortunately, in the dilute limit, it can be factorized a similar way to that of the two-body case in Eq. (10),

$$\varphi(x_\downarrow; x_\uparrow) = \det\left(e^{i\chi_{i_1} x_{i_2}}\right) \det\left(e^{i\chi_{j_1} x_{j_2}}\right) e^{-\frac{1}{2}\sum_{ij} W(x_{ij})}, \quad (16)$$

in which two $\det(\cdots)$ represent the Slater determinants of the plane waves for spin-up and down particles, respectively; the two-body Jastrow factor in Eq. (10) is also generalized to the many-body case. Here $1 \le i, i_1, i_2 \le N_\downarrow$ and $N_\downarrow + 1 \le j, j_1, j_2 \le N$ are the coordinate indexes for spin-down and up particles, respectively, and $x_{ij} = x_i - x_j$ represents the distance between them. This wave function is similar to that of the Hubbard model at $U \to \infty$ [37], where the BA wave function is factorized into a Slater determinaint of spinless fermions and a BA wave function of the spin-1/2 chain.

The above simplification is justified as follows. As illustrated in Fig. 2, the wave function is approximated to a summation of incident waves with different coordinate permutations. In other words,

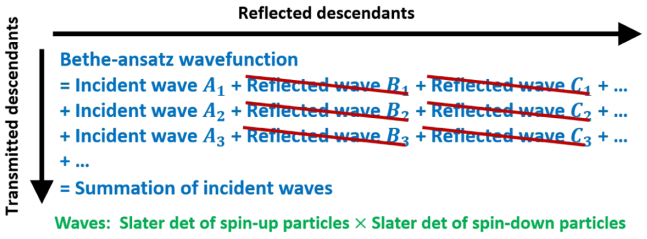

FIG. 2. The construction of the Bethe-ansatz wave function. It is composed of many "plane waves." Each plane wave is a product of Slater determinants, due to the Fermi statistics. The "plane waves" in the same column or the same row are connected by transmission or reflection, respectively. Due to the diffractive reflection described by Eq. (9), the reflected descendants of A_i are all suppressed.

$$\varphi(x_\downarrow; x_\uparrow) = \det\left(e^{i\chi_{i_1} x_{i_2}}\right) \det\left(e^{i\chi_{j_1} x_{j_2}}\right) e^{-\sum_{ij} \frac{\eta_r x_{ij}}{L}} \times \sum_Q \theta(x_{Q_1} > x_{Q_2} > \cdots > x_{Q_N}) A(Q),$$

where Q represents the permutation $x_{Q_1} > x_{Q_2} > \cdots > x_{Q_N}$ with $1 \le Q_l \le N$. $\sum_Q$ denotes the sum over all permutations. These incident waves differ by a "phase shift" whose module is not 1 due to the non-Hermitian SOC. After switching a pair of neighboring particles with opposite spins, the amplitudes are changed by

$$\frac{A(\cdots\uparrow\downarrow\cdots)}{A(\cdots\downarrow\uparrow\cdots)} = 1 + \frac{g}{\alpha} + O\left(\frac{\lambda_s}{d}\right), \quad (17)$$

which is momentum independent at the leading order. As proved in SM Sec. II [44], in this case the summation of step functions can be organized into

$$\sum_Q \theta(x_{Q_1} > x_{Q_2} > \cdots > x_{Q_N}) A(Q) = e^{-\eta_r \sum_{ij} \theta(x_j - x_i)}.$$

Further simplification yields the wave function Eq. (16).

Application—As an application of the above solution, we identify a phase transition in our system. Consider the case with an equal number of spin-up and spin-down particles, whose real parts of the momenta are $2\pi n_l/L$. Without loss of generality, assume the particle numbers of both components are odd. The quantum numbers n_j and n_i for spin-up and down particles take the values of

$$-\frac{N-2}{4}, -\frac{N-6}{4}, \cdots -1, 0, 1, \ldots \frac{N-6}{4}, \frac{N-2}{4}.$$

In this case, the Slater determinant simplifies to [47]

$$\det\left(e^{i\chi_{i_1} x_{i_2}}\right) = \prod_{i_1 < i_2} \left(2i \sin\frac{\pi(x_{i_1} - x_{i_2})}{L}\right).$$

The probability distribution function $|\varphi(x_\downarrow; x_\uparrow)|^2$ can be expressed as a thermodynamic distribution, similar to the case of the Laughlin wave function [38]:

$$|\varphi(x_\downarrow; x_\uparrow)|^2 = \rho(x_\downarrow; x_\uparrow) = e^{-\mathcal{H}}. \quad (18)$$

The effective Hamiltonian $\mathcal{H}$ is

$$\mathcal{H} = \sum_{i_1 < i_2} V(x_{i_1, i_2}) + \sum_{j_1 < j_2} V(x_{j_1, j_2}) + \sum_{ij} W(x_{ij}), \quad (19)$$

where $x_{i_1,i_2} = x_{i_1} - x_{i_2}$ and $x_{j_1,j_2} = x_{j_1} - x_{j_2}$. $V(r) = -2\ln\left|\sin(\pi/L)r\right|$ originates from the Pauli exclusion principle, which describes an effective repulsion between particles of identical spins; W brings a unidirectional

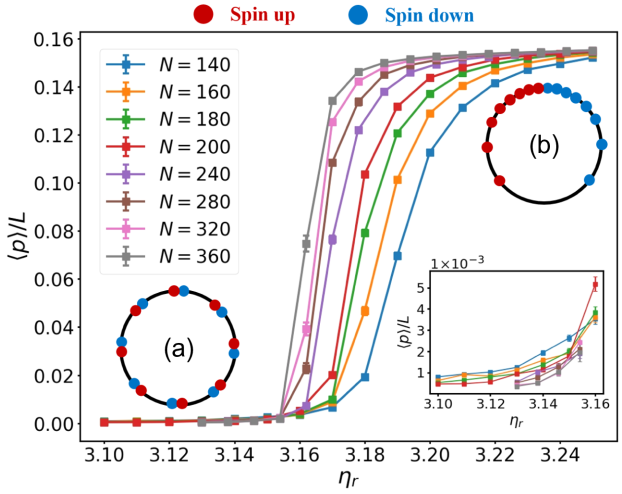

FIG. 3. The Monte Carlo simulations of the average "spin dipole" $\langle p\rangle$ at $L = 100$ with different particle numbers. As $\eta_r = \ln(1 + g/\alpha)$ increases, $\langle p\rangle/L$ jumps from zero to a finite value, indicating that the transition is of first order. (a),(b) shows the configuration of the two phases. If α is fixed, the more localized (b) phase emerges only when g is big enough, which implies that the many-body resonance is enhanced by the repulsive interaction.

attraction between opposite spins, with spin-up particles preferring the left side of spin-down ones.

If V dominates, particles tend to uniformly distribute along the ring, with a weak pairing tendency between opposite spins to take the advantage of W, as depicted in Fig. 3(a). Conversely, if W dominates, the system prefers phase separation, such that nearly all spin-up particles lie on the left of spin-down particles, making the configuration in Fig. 3(b) more favorable. The competition between V and W is investigated via Monte Carlo simulations with the probability distribution Eq. (18). We consider the "dipole" strength $p = [1/(N/2)^2]\sum_{ij} p_{ij}$, where p_{ij} is the dipole between a spin-down and up particle located at x_i and x_j, respectively,

$$p_{ij} = \begin{cases} x_{ij}, & |x_{ij}| \le L/2, \\ x_{ij} - \mathrm{sgn}(x_{ij})L, & |x_{ij}| > L/2. \end{cases} \tag{20}$$

With this definition, $-L/2 < p \le L/2$. The thermodynamics average $\langle p\rangle$ is plotted in Fig. 3. As η_r increases, $\langle p\rangle/L$ evolves from zero, which is consistent with Fig. 3(a), to a finite value, illustrated in Fig. 3(b). The transition takes places at $\eta_r \approx 3.15$. Note that η_r measures the strength of resonance, which is enhanced by the repulsive interaction as shown in the two-body case. Therefore, the emergence of the (b) phase demonstrates a many-body "skin effect" driven by the repulsive interaction, which is in stark contrast to the conventional NHSE [32–36].

The abrupt change of the dipole strength p at the transition point indicates a first-order phase transition. Let us gain a better understanding by introducing an effective "temperature" defined as

$$\rho_\beta = e^{-\beta\mathcal{H}},$$

in which $\beta = 1$ corresponds to the situation described by Eq. (18). Consider the zero-temperature limit $\beta \to \infty$ such that the system freezees into the minimal energy configuration of $\mathcal{H}$. As an example, we examine the case of four particles shown in SM Sec. III [44]. The energy minima at small and large values of η_r are calculated, which correspond to frozen configurations shown in Figs. 3(a) and 3(b), respectively. The switch of minima occurs at $\eta_r = 3.84$, roughly matching the transition point shown in Fig. 3.

Discussion and conclusion—We present a BA solution to a 1D interacting spin-1/2 non-Hermitian system breaking the inversion symmetry. The interplay between non-Hermitian SOC and the repulsive interaction results in a novel many-body resonance state. The complicated BA wave function is simplified in the dilute limit, which is cast into the Slater-Jastrow form. Its amplitude square is mapped into a thermodynamic distribution, exhibiting the competition between Pauli's exclusion among fermions of the same component and resonances between fermions of different components. The former brings a repulsion and the latter generates an unidirectional attraction. This competition leads to a transition from a uniform configuration with weak pairing tendency to a phase separation, showing that the many-body resonance is enhanced by the repulsive interaction.

Acknowledgments—We are grateful to K. Yang, W. Yang, J. D. Wu, and C. H. Ke for valuable discussions. C. W. is supported by the National Natural Science Foundation of China under (Grants No. 12234016, No. 12574274, and No. 12550402). Z. Y. is supported by the National Key Research and Development Program of China (Grant No. 2023YFA1407500), the National Natural Science Foundation of China (Grant No. 12322405), and the Fundamental Research Funds for the Central Universities (20720230011). This work has been supported by the New Cornerstone Science Foundation.

Data availability—The data that support the findings of this article are not publicly available upon publication because it is not technically feasible and/or the cost of preparing, depositing, and hosting the data would be prohibitive within the terms of this research project. The data are available from the authors upon reasonable request.

[1] T. E. Lee, Anomalous edge state in a non-Hermitian lattice, Phys. Rev. Lett. **116**, 133903 (2016).
[2] V. M. Martinez Alvarez, J. E. Barrios Vargas, and L. E. F. Foa Torres, Non-Hermitian robust edge states in one dimension:

Anomalous localization and eigenspace condensation at exceptional points, Phys. Rev. B **97**, 121401(R) (2018).
[3] S. Yao and Z. Wang, Edge states and topological invariants of non-Hermitian systems, Phys. Rev. Lett. **121**, 086803 (2018).
[4] C. H. Lee, L. Li, and J. Gong, Hybrid higher-order skin-topological modes in nonreciprocal systems, Phys. Rev. Lett. **123**, 016805 (2019).
[5] C. H. Lee and R. Thomale, Anatomy of skin modes and topology in non-Hermitian systems, Phys. Rev. B **99**, 201103(R) (2019).
[6] D. S. Borgnia, A. J. Kruchkov, and R.-J. Slager, Non-Hermitian boundary modes and topology, Phys. Rev. Lett. **124**, 056802 (2020).
[7] X.-R. Wang, C.-X. Guo, and S.-P. Kou, Defective edge states and number-anomalous bulk-boundary correspondence in non-Hermitian topological systems, Phys. Rev. B **101**, 121116(R) (2020).
[8] X.-R. Ma, K. Cao, X.-R. Wang, Z. Wei, Q. Du, and S.-P. Kou, Non-Hermitian chiral skin effect, Phys. Rev. Res. **6**, 013213 (2024).
[9] F. K. Kunst, E. Edvardsson, J. C. Budich, and E. J. Bergholtz, Biorthogonal bulk-boundary correspondence in non-Hermitian systems, Phys. Rev. Lett. **121**, 026808 (2018).
[10] K. Yokomizo and S. Murakami, Non-Bloch band theory of non-Hermitian systems, Phys. Rev. Lett. **123**, 066404 (2019).
[11] Z. Yang, K. Zhang, C. Fang, and J. Hu, Non-Hermitian bulk-boundary correspondence and auxiliary generalized brillouin zone theory, Phys. Rev. Lett. **125**, 226402 (2020).
[12] S. Yao, F. Song, and Z. Wang, Non-Hermitian Chern bands, Phys. Rev. Lett. **121**, 136802 (2018).
[13] F. Song, S. Yao, and Z. Wang, Non-Hermitian skin effect and chiral damping in open quantum systems, Phys. Rev. Lett. **123**, 170401 (2019).
[14] K. Zhang, Z. Yang, and C. Fang, Correspondence between winding numbers and skin modes in non-Hermitian systems, Phys. Rev. Lett. **125**, 126402 (2020).
[15] M. Brandenbourger, X. Locsin, E. Lerner, and C. Coulais, Non-reciprocal robotic metamaterials, Nat. Commun. **10**, 4608 (2019).
[16] A. Ghatak, M. Brandenbourger, J. Van Wezel, and C. Coulais, Observation of non-Hermitian topology and its bulk–edge correspondence in an active mechanical metamaterial, Proc. Natl. Acad. Sci. U.S.A. **117**, 29561 (2020).
[17] L. Xiao, T. Deng, K. Wang, G. Zhu, Z. Wang, W. Yi, and P. Xue, Non-Hermitian bulk–boundary correspondence in quantum dynamics, Nat. Phys. **16**, 761 (2020).
[18] T. Hofmann, T. Helbig, F. Schindler, N. Salgo, M. Brzezińska, M. Greiter, T. Kiessling, D. Wolf, A. Vollhardt, A. Kabaši, C. H. Lee, A. Bilušić, R. Thomale, and T. Neupert, Reciprocal skin effect and its realization in a topolectrical circuit, Phys. Rev. Res. **2**, 023265 (2020).
[19] S. Liu, R. Shao, S. Ma, L. Zhang, O. You, H. Wu, Y. J. Xiang, T. J. Cui, and S. Zhang, Non-Hermitian skin effect in a non-Hermitian electrical circuit, Research **2021**, 5608038 (2021).
[20] L. Zhang, Y. Yang, Y. Ge, Y.-J. Guan, Q. Chen, Q. Yan, F. Chen, R. Xi, Y. Li, D. Jia *et al.*, Acoustic non-Hermitian skin effect from twisted winding topology, Nat. Commun. **12**, 6297 (2021).
[21] Q. Liang, D. Xie, Z. Dong, H. Li, H. Li, B. Gadway, W. Yi, and B. Yan, Dynamic signatures of non-Hermitian skin effect and topology in ultracold atoms, Phys. Rev. Lett. **129**, 070401 (2022).
[22] V. E. Korepin, V. E. Korepin, N. Bogoliubov, and A. Izergin, *Quantum Inverse Scattering Method and Correlation Functions* (Cambridge University Press, Cambridge, England, 1997), Vol. 3, 10.1017/CBO9780511628832.
[23] Y. Wang, W.-L. Yang, J. Cao, and K. Shi, *Off-Diagonal Bethe Ansatz for Exactly Solvable Models* (Springer, New York, 2015), 10.1007/978-3-662-46756-5.
[24] E. H. Lieb and W. Liniger, Exact analysis of an interacting Bose gas. I. The general solution and the ground state, Phys. Rev. **130**, 1605 (1963).
[25] E. H. Lieb, Exact analysis of an interacting Bose gas. II. The excitation spectrum, Phys. Rev. **130**, 1616 (1963).
[26] C. N. Yang, Some exact results for the many-body problem in one dimension with repulsive delta-function interaction, Phys. Rev. Lett. **19**, 1312 (1967).
[27] M. Gaudin, Un systeme a une dimension de fermions en interaction, Phys. Lett. **24A**, 55 (1967).
[28] E. H. Lieb and F. Y. Wu, Absence of Mott transition in an exact solution of the short-range, one-band model in one dimension, Phys. Rev. Lett. **20**, 1445 (1968).
[29] A. A. Ziolkowska and F. H. Essler, Yang-Baxter integrable Lindblad equations, SciPost Phys. **8**, 044 (2020).
[30] B. Buča, C. Booker, M. Medenjak, and D. Jaksch, Bethe ansatz approach for dissipation: Exact solutions of quantum many-body dynamics under loss, New J. Phys. **22**, 123040 (2020).
[31] C. Ekman and E. J. Bergholtz, Liouvillian skin effects and fragmented condensates in an integrable dissipative Bose-Hubbard model, Phys. Rev. Res. **6**, L032067 (2024).
[32] M. Nakagawa, N. Kawakami, and M. Ueda, Exact Liouvillian spectrum of a one-dimensional dissipative Hubbard model, Phys. Rev. Lett. **126**, 110404 (2021).
[33] L. Mao, Y. Hao, and L. Pan, Non-Hermitian skin effect in a one-dimensional interacting Bose gas, Phys. Rev. A **107**, 043315 (2023).
[34] H.-R. Wang, B. Li, F. Song, and Z. Wang, Scale-free non-Hermitian skin effect in a boundary-dissipated spin chain, SciPost Phys. **15**, 191 (2023).
[35] P. Kattel, P. R. Pasnoori, and N. Andrei, Exact solution of a non-Hermitian PT-symmetric spin chain, J. Phys. A **56**, 325001 (2023).
[36] M. Zheng, Y. Qiao, Y. Wang, J. Cao, and S. Chen, Exact solution of the Bose-Hubbard model with unidirectional hopping, Phys. Rev. Lett. **132**, 086502 (2024).
[37] M. Ogata and H. Shiba, Bethe-ansatz wave function, momentum distribution, and spin correlation in the one-dimensional strongly correlated Hubbard model, Phys. Rev. B **41**, 2326 (1990).
[38] R. B. Laughlin, Anomalous quantum Hall effect: An incompressible quantum fluid with fractionally charged excitations, Phys. Rev. Lett. **50**, 1395 (1983).
[39] M. Girardeau, Relationship between systems of impenetrable bosons and fermions in one dimension, J. Math. Phys. (N.Y.) **1**, 516 (1960).
[40] W. Yang, J. Wu, S. Xu, Z. Wang, and C. Wu, One-dimensional quantum spin dynamics of Bethe string states, Phys. Rev. B **100**, 184406 (2019).
[41] Z. Wang, J. Wu, W. Yang, A. K. Bera, D. Kamenskyi, A. N. Islam, S. Xu, J. M. Law, B. Lake, C. Wu *et al.*, Experimental

observation of Bethe strings, Nature (London) **554**, 219 (2018).
[42] M. Takahashi, *Thermodynamics of One-Dimensional Solvable Models* (Cambridge University Press, Cambridge, England, 1999), 10.1017/CBO9780511524332.
[43] R. Jastrow, Many-body problem with strong forces, Phys. Rev. **98**, 1479 (1955).
[44] See Supplemental Material at http://link.aps.org/supplemental/10.1103/bhpz-17d2, which contains the following information: the solution to the two-body problem, a detailed treatment to the Bethe-Ansatz equations and a justification of the simplified many-body wavefunction in the dilute limit, a demonstration of transition in the 4-particle case, and a discussion of the experimental realization in lattice with pure loss.
[45] L. Li, C. H. Lee, S. Mu, and J. Gong, Critical non-Hermitian skin effect, Nat. Commun. **11**, 5491 (2020).
[46] L. Li, C. H. Lee, and J. Gong, Impurity induced scale-free localization, Commun. Phys. **4**, 42 (2021).
[47] C. Gros, R. Joynt, and T. M. Rice, Antiferromagnetic correlations in almost-localized Fermi liquids, Phys. Rev. B **36**, 381 (1987).
[48] Y. Yi and Z. Yang, Non-Hermitian skin modes induced by on-site dissipations and chiral tunneling effect, Phys. Rev. Lett. **125**, 186802 (2020).
[49] B. Buča, C. Booker, M. Medenjak, and D. Jaksch, Bethe ansatz approach for dissipation: Exact solutions of quantum many-body dynamics under loss, New J. Phys. **22**, 123040 (2020).

End Matter

As for experimental realizations, a 1D lattice Hamiltonian was proposed in [48], in which the spin-dependent coupling between two sublattices transfers the onsite loss into the non-Hermitian SOC studied in our work. Upon open boundary conditions, it exhibits a spin-dependent NHSE, which is a signature of the non-Hermitian SOC (more details are presented in SM Sec. IV [44]). It is expected that upon turning on repulsions and switching to the periodical boundary condition, such a system will exhibit the many-body resonance effect qualitatively similar to what we have studied. Due to the sublattice structure, such a model is no longer integrable. Further numerical investigations are deferred to a later publication.

For realistic experimental systems with pure loss, the dynamics should be governed by the Lindblad equation, which is more challenging to solve compared to the non-Hermitian Hamiltonian. Full treatment of this problem will be deferred to future publication. Nevertheless, we believe that the resonance effect derived from the many-body wave function Eq. (16) is robust enough even under particle loss. The key point is that the many-body resonance we identify is not a property of a single many-body eigenstate but is instead shared by all eigenstates. The robustness of the many-body resonance is also evident within the Lindbladian formalism. For purely lossy systems, the eigenmodes of the Lindblad superoperator are linear combinations of the basis constructed by the eigenstates of the corresponding non-Hermitian Hamiltonian [49]. Supposition of states within the same particle-number sector preserve the resonance effect, since all the eigenstates share a common Jastrow factor. As shown in Eq. (16), the Jastrow factor is only determined by the numbers of spin-up and spin-down particles and is independent of the Bethe Ansatz quantum numbers. As the particle number decays over time, it should exhibit a distribution at each time. Because states in different particle-number sectors do not have spatial interference, the resonance effect is dominated by the most probable sectors of particle numbers. Therefore, the resonance effect should persist during particle loss, with quantitative modifications determined by the level particle-number fluctuations.